THE JOURNAL OF BIOLOGICAL CHEMISTRY
Vol. 279, No. 5, Issue of January 30, pp. 3361–3369, 2004

Printed in U.S.A.

Amyloid Nucleation and Hierarchical Assembly of Ure2p Fibrils

ROLE OF ASPARAGINE/GLUTAMINE REPEAT AND NONREPEAT REGIONS OF THE PRION DOMAIN*

Received for publication, September 22, 2003, and in revised form, November 4, 2003
Published, JBC Papers in Press, November 10, 2003, DOI 10.1074/jbc.M310494200

Yi Jiang‡, Hui Li§, Li Zhu‡, Jun-Mei Zhou‡¶, and Sarah Perrett‡¶‖

From the ‡National Laboratory of Biomacromolecules, Institute of Biophysics, Chinese Academy of Sciences, 15 Datun Road, Chaoyang District, Beijing 100101, and the §State Key Laboratory of Magnetism, Center for Condensed Matter Physics, Institute of Physics, Chinese Academy of Sciences, P. O. Box 603, Beijing 100080, China

The yeast prion protein Ure2 forms amyloid-like filaments *in vivo* and *in vitro*. This ability depends on the N-terminal prion domain, which contains Asn/Gln repeats, a motif thought to cause human disease by forming stable protein aggregates. The Asn/Gln region of the Ure2p prion domain extends to residue 89, but residues 15–42 represent an island of "normal" random sequence, which is highly conserved in related species and is relatively hydrophobic. We compare the time course of structural changes monitored by thioflavin T (ThT) binding fluorescence and atomic force microscopy for Ure2 and a series of prion domain mutants under a range of conditions. Atomic force microscopy height images at successive time points during a single growth experiment showed the sequential appearance of at least four fibril types that could be readily differentiated by height (5, 8, 12, or 9 nm), morphology (twisted or smooth), and/or time of appearance (early or late in the plateau phase of ThT binding). The Ure2 dimer (h = 2.6 ± 0.5 nm) and granular particles corresponding to higher order oligomers (h = 4–12 nm) could also be detected. The mutants 15Ure2 and Δ15–42Ure2 showed the same time-dependent variation in fibril types but with an increased lag time detected by ThT binding compared with wild-type Ure2. In addition, Δ15–42Ure2 showed reduced binding to ThT. The results imply a role of the conserved region in both amyloid nucleation and formation of the binding surface recognized by ThT. Further, Ure2 amyloid formation is a multistep process via a series of fibrillar intermediates.

Ure2p is the protein determinant of the epigenetic factor [URE3] of *Saccharomyces cerevisiae*, which has been demonstrated to represent a prion of yeast (1, 2). Analogous to the mammalian prion protein (3), Ure2p is aggregated, inactive, and protease-resistant in prion strains (1, 2). In addition, amyloid-like filaments are observed both *in vivo* (4) and *in vitro* (5, 6). Fibrils formed *in vitro* show characteristic green birefringence on Congo red binding (5, 7, 8) and also bind thioflavin T (ThT)[1] (7–9), a dye considered highly specific for amyloid (10, 11). Amyloids are thought to form by conversion of the native protein structure to a generic cross-β structure, identified by a characteristic x-ray diffraction pattern (12). However, an unusual property of Ure2 fibrils is their ability to maintain native-like ligand binding properties within the fibrillar arrays (8, 13). Consistent with this, Ure2 fibrils formed by standing at subambient temperatures show a Fourier transform infrared spectrum consistent with native-like helical content (8), and the cross-β x-ray diffraction band becomes apparent only after incubation of the protein close to the T_m (14). Atomic force microscopy (AFM) imaging of these "native-like" fibrils shows them to be homogeneous, with a height of around 12 nm and a periodicity of around 50 nm (8).

Ure2 prion formation *in vivo* (2) and fibril formation *in vitro* (5, 15) are dependent on the presence of the N-terminal ~90 amino acids. The N-terminal prion domain (PrD) is unstructured in the native state (6, 16) and is rich in Asn and Gln residues (see Fig. 1). Deletion of all or parts of the PrD has no discernible effect on the dimeric structure, thermodynamic stability, folding kinetics, or folding pathway of Ure2 under a wide range of conditions (9, 15, 16, 20–22). Expansion of Gln (or CAG) repeats is responsible for a number of human neurodegenerative diseases, including Huntington's disease (23). The ability of poly-Gln or poly-Asn regions to aggregate by forming a hydrogen bonded β-sheet structure is thought to cause disease (24–27), either by direct toxicity (28) or by sequestration of other vital cellular proteins (29, 30). There is evidence for poly-Gln and other amyloid diseases that the species most damaging to cells are protofibrils, or intermediates formed early in the aggregation process, rather than large fibrillar aggregates (31, 32).

ThT binding provides a convenient method to measure the effect of different environmental factors on the kinetics of amyloid formation (9, 33). The time course of Ure2 amyloid formation monitored by ThT binding shows a sigmoidal curve, representing a lag time, an exponential growth phase, and a plateau region (7–9). The lag time can be circumvented by seeding with preformed amyloid-like fibrils (5–7) and is protein concentration-dependent (6, 9). This is consistent with a nucleation-dependent mechanism (34, 35), where the lag time reflects the kinetic barrier to association of a sufficient number of molecules to form a thermodynamically stable nucleus or seed. However, once this stable nucleus is formed, exponential growth from the fibril ends is then observed, until steady-state conditions are reached. Results from a number of laboratories indicate that conditions that produce this characteristic increase in dye binding for Ure2

* This work was supported in part by Natural Science Foundation of China Grant 30070163, 973 Project of the Chinese Ministry of Science and Technology G1999075608, and State Key Development Plan Project 199801012. The costs of publication of this article were defrayed in part by the payment of page charges. This article must therefore be hereby marked "*advertisement*" in accordance with 18 U.S.C. Section 1734 solely to indicate this fact.

¶ To whom correspondence may be addressed. Tel.: 86-10-6488-8496; Fax: 86-10-6484-0672; E-mail: zhoujm@sun5.ibp.ac.cn or sarah.perrett@iname.com.

‖ Supported by the Chinese Academy of Sciences, the Royal Commission for the Exhibition of 1851, and the Royal Society.

[1] The abbreviations used are: ThT, thioflavin T; AFM, atomic force spectroscopy; EM, electron microscopy; PrD, prion domain; WT, wild-type.

also lead to the eventual appearance of well formed amyloid-like fibrils, visualized by EM or AFM (5–9). Oligomeric particles or rods of Ure2 have been observed by EM (6) and AFM (8). However, the relationship between the time course of changes in ThT binding and evolution of amyloid-like structure has not been investigated for Ure2. AFM offers particular advantages over EM, in that hydrated samples can be observed directly, in air, without requirement for staining. In addition, AFM can detect the presence of aggregated species as well as differences in fibril morphology which are not apparent in EM images (8, 36, 37).

Here we compare the time course of structural changes monitored by ThT binding and AFM and examine the role of different parts of the Ure2 PrD sequence on the kinetics of fibril formation.

EXPERIMENTAL PROCEDURES

Materials—ThT and Tris were from Sigma. Ure2 and N-terminal variants, 15Ure2, Δ15–42Ure2, 42Ure2, and 90Ure2 (see Fig. 1) were produced in *Escherichia coli* with a short His tag and purified as described previously (9, 16). 42Ure2 was constructed as described previously for the other mutants (16). Proteins were stored at −80 °C and defrosted in a 25 °C water bath immediately prior to use. Samples were prepared in 50 mM KH_2PO_4-Na_2HPO_4 buffer containing 0.15 M NaCl, or in 50 mM Tris-HCl buffer containing 0.2 M NaCl as described (9) and centrifuged at 18,000 × *g* for 30 min at 4 °C to remove any aggregated protein.

Amyloid Formation—The kinetics of amyloid formation of Ure2 proteins was monitored using ThT binding fluorescence as described previously (7, 9, 33, 38). Incubation was at a constant temperature of 25 or 37 °C with shaking, as described previously (9). Alternatively, proteins were incubated without shaking at 4 or 25 °C. NaN_3 (0.02% w/v) was added to prevent bacterial growth. The pH range of buffers used was 7.5–8.4 (at 25 °C), and the protein concentration range was 15–40 μM for full-length Ure2 and 30–140 μM for Ure2 mutants. The pH values given in the text are correct at the temperature of incubation, allowing for the temperature dependence of the pH of Tris buffer. At regular time intervals, 10-μl aliquots were removed from the reaction mixture and assayed for ThT binding, as described previously (9). Samples were incubated in parallel whenever possible. When comparing the time course of amyloid formation by ThT binding and AFM, samples were taken simultaneously from the same reaction vessel whenever possible.

AFM—A 10-μl drop of the protein sample was deposited on freshly cleaved mica, allowed to stand for 10 min in air, then washed with three 200-μl aliquots of distilled deionized water, before drying for 4 min in a stream of nitrogen. Tapping mode AFM was performed using a Nanoscope IIIa Multimode-AFM instrument (Digital Instruments) under ambient conditions. Super-sharp silicon tips (Silicon-MDT Ltd.) with resonance frequency of about 106 kHz were used at a scan rate of 1–2 Hz. Once the tip was engaged, the set point value was adjusted to minimize the force exerted on the sample while maintaining the sharpness of the image.

Height measurements of granular and fibrillar particles were performed manually using the software provided with the Nanoscope instrument. To compare the size distribution of granules over time, the maximal height of every granular particle detected within a representative scan area of fixed size was measured for each time point. To determine the distribution of heights of fibrils, the height profiles were measured perpendicular to the fibril over a region greater than the periodicity of height variations within an individual fibril. The average peak height for each fibril was recorded (maximal variation around 1 nm). Mean heights were obtained by fitting to a Gaussian curve. The errors shown are the standard deviation.

Scanning different regions of the mica surface confirmed that the distribution of particles or fibrils was uniform and that the scan areas sampled were representative, with the exception that protofilaments were deposited preferentially at the edge of the grids, suggesting that they are more easily dislodged from the mica surface by the washing process than mature fibrils. This has important consequences for the interpretation of the data because it indicates that although protofilament formation clearly precedes fibril formation, protofilaments are present earlier and more abundantly than apparent from the AFM assay procedure. This may explain in part the increased tendency to observe protofilaments when fibrils are grown *in situ* on the mica (39).

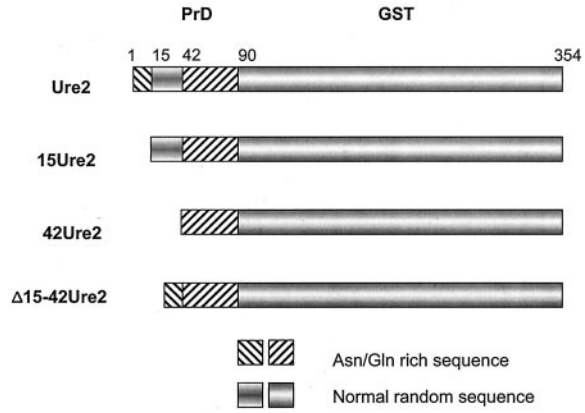

FIG. 1. **Primary structure of the Ure2p N-terminal PrD in the WT protein and in the prion domain deletion mutants.** Repetitive regions detected by sequence analysis (16) are indicated by *diagonal stripes* or *bold type*. Hydrophobic regions of the PrD, identified by plotting the relative hydrophobicity (17, 18), are *underlined*. The C-terminal region has homology to the glutathione *S*-transferase protein family (19).

RESULTS

Ure2 Mutants 15Ure2 and Δ15–42Ure2 Show an Increase in the Lag Time Detected by ThT Binding—ThT binding provides a convenient method to assay the effect of different factors on the kinetics of amyloid formation (9, 33). We compared the ThT-monitored kinetics of amyloid formation for full-length Ure2 and a series of PrD deletion mutants. The mutants examined were 15Ure2, which lacks the first stretch of repetitive sequence; Δ15–42Ure2, which retains all the Asn/Gln repeat regions, but lacks the island of "normal" random sequence within the PrD; 42Ure2, which lacks the first 41 residues of the PrD; and 90Ure2, in which the entire Asn/Gln repeat region has been deleted (Fig. 1). The WT and mutant Ure2 proteins were compared under a range of incubation conditions, including different temperatures (4, 25, and 37 °C), buffer systems (sodium/potassium phosphate or Tris-HCl), and with or without agitation. Representative curves for a variety of conditions are shown in Fig. 2. The mutants 42Ure2 and 90Ure2 showed a negligible increase in ThT binding fluorescence even at maximal protein concentrations. This is consistent with the requirement of residues 1–65 for induction or maintenance of the prion state *in vivo* (2, 40). Interestingly, the mutant 15Ure2 consistently showed a sigmoidal time course monitored by ThT binding, similar to that for WT Ure2, but with a longer lag time (Fig. 2). Δ15–42Ure2 showed greatly reduced binding to ThT compared with 15Ure2 or WT. However, under certain conditions (particularly in Tris buffer at relatively high protein concentrations), the limited increase in ThT binding for Δ15–42Ure2 could be seen to be sigmoidal, revealing a lag time slower than for WT Ure2 and similar to 15Ure2 at the same protein concentration (Fig. 2*B*). This suggests a role of both Asn/Gln repeat (residues 1–14) and nonrepeat (residues 15–42) regions of the PrD in nucleation of amyloid structure. However, it also indicates that deletion of either one of these two regions does not ablate the ability to form an amyloid-like structure.

Characterization of the Ure2 Dimer by AFM—AFM height imaging provides a convenient method to characterize the morphology of biological macromolecules at submolecular resolution without requirement for staining (36, 37, 39, 41–43). Typ-

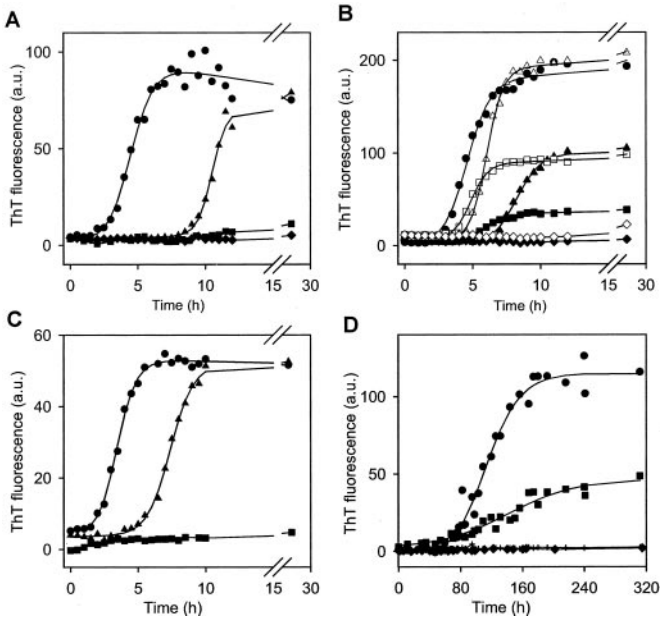

FIG. 2. **Kinetics of formation of amyloid-like structure for Ure2 and PrD mutants monitored by ThT binding under a range of conditions.** Values of pH are correct at the temperature of incubation. *A*, 40 μM Ure2 (●), 15Ure2 (▲), Δ15–42Ure2 (■), and 42Ure2 (♦) incubated in Tris-HCl buffer, pH 7.5, 0.2 M NaCl at 25 °C with shaking. *B*, 30 μM Ure2 (●); 40 μM (▲) and 80 μM (△) 15Ure2; 40 μM (■) and 80 μM (□) Δ15–42Ure2; and 40 μM (♦) and 80 μM (◇) 42Ure2 incubated in Tris-HCl buffer, pH 7.2, 0.2 M NaCl at 37 °C with shaking. *C*, 30 μM Ure2 (●), 40 μM 15Ure2 (▲), and 80 μM Δ15–42Ure2 (■) incubated in sodium/potassium phosphate buffer, pH 8.0, 0.2 M NaCl at 37 °C with shaking. *D*, 40 μM Ure2 (●), Δ15–42Ure2 (■), 42Ure2 (♦), and 90Ure2 (+) incubated in Tris-HCl buffer, pH 9.0, 0.2 M NaCl at 4 °C without shaking.

ically, the sample is adsorbed onto mica, and the surface is scanned with an oscillating or "tapping" tip on a microcantilever. The variations in height can then be represented by a gray scale, ranging from white (high) to black (low), to form the image. A characteristic of AFM imaging is that the size of the scanning tip relative to the size of protein oligomers or fibrils results in an overestimation of the width, whereas the height of the sample above the mica surface can be measured with accuracy and reproducibility. Nevertheless, the height of biological molecules measured by AFM tends to be smaller than the diameter measured by other structural methods, which may reflect the absence of stain, the degree of hydration, and/or compression by the AFM tip.

To calibrate the height of the Ure2 dimer by AFM, we prepared a series of dilutions of Ure2 and the mutants Δ15–42Ure2 and 90Ure2 in Tris-HCl buffer, pH 8.4, 0.2 M NaCl at 25 °C. Under these conditions the protein shows a minimal tendency to aggregate and is expected to be predominantly dimeric at micromolar protein concentrations (16), although species with sedimentation values corresponding to monomers and tetramers are detected under similar buffer conditions at 15 °C, depending on the protein concentration (6). After adsorption of a 1 μM protein solution of WT or mutant Ure2 onto mica, AFM imaging reveals a homogenous population of spherical particles (Fig. 3). The predominant species has a height of 2.6 ± 0.5 nm (Fig. 3*C*, *upper panel*). The WT sample contained a minor population (less than 5%) of larger particles (Fig. 3*A*), which have heights in the range 4–8 nm (data not shown). At lower protein concentrations, an additional peak at 1.3 ± 0.3 nm appears (Fig. 3*C*, *lower panel*), consistent with population of the monomer. Identical peaks are observed for WT Ure2, Δ15–42Ure2, and 90Ure2, indicating that the PrD does not contribute to the height of the Ure2 monomer or dimer as measured by AFM.

Comparison of Time Course of Structural Changes Monitored by ThT Binding and AFM—To ascertain the structural basis of the differences in kinetics detected by ThT binding for Ure2 and the PrD mutants described above, we measured the time course of structural changes in parallel by ThT binding and tapping mode AFM. In each case, aliquots were removed from the reaction vessel for assay. Fig. 4 shows a comparison of the time course measured by the two methods for Ure2 incubated in phosphate buffer, pH 8.0, at 37 °C with shaking. Under these conditions, abundant well formed fibrils are formed within 24 h, as detected by EM, and the time course of ThT binding is highly reproducible and relatively rapid (9), so that a plateau is reached within 12 h (Fig. 4*A*). The initial Ure2 protein solution was found to contain a variety of sizes of granular particles (Fig. 4, *B* and *E*, *0 h*), ranging in height from 1 to 85 nm, although greater than 90% of the particles were less than 20 nm in height. The larger particles appear to be dispersed or precipitated after the onset of shaking and are concluded to represent amorphous aggregates. Occasional fibrillar structures are also detected in the initial sample (Fig. 4*E*, *0 h*). The presence of a low concentration of preformed fibrils, or nuclei for fibril formation, could account for the linear rather than exponential dependence of the lag time on initial Ure2 concentration, as discussed previously (9).

Changes in the height distribution of granular particles over the time course of the ThT-monitored curve were examined by recording the heights of all granules within a representative 2-μm square at hourly time points between the onset of incubation (0 h) and the onset of fibril formation (7 h). Within the lag phase region (0–2 h), there was a marked increase in the number of particles of height 4–6 nm, which was then followed (2–3 h) by an increase in particles of height 8–12 nm (Fig. 4*C*), coinciding with an increase in ThT binding fluorescence (Fig. 4*A*). Given the height of the Ure2 dimer of 2.6 ± 0.5 nm (Fig. 3), this then suggests that the 4–6-nm particles that appear during the lag phase are tetramers or hexamers, whereas the 8–12-nm particles are likely to represent larger oligomers.

The earliest fibril-like structures appear late in the exponential phase of ThT binding (6 h) and have a height of around 5 nm, thus resembling the protofilaments observed for other amyloidogenic proteins (28, 31, 36, 37, 39, 42, 43). These are succeeded by 8-nm fibrils (7 h) and then 12-nm fibrils (8 h). Significant numbers of fibrillar structures are not detected until ThT binding has already reached a plateau (Fig. 4, *A*, *D*, and *E*). However, the number of protofilaments is underestimated in the AFM assay (see "Experimental Procedures"). It is therefore likely that both protofilaments (5 nm; also 2.5 nm, see below) and larger granules (8–12 nm) contribute to the onset of ThT binding.

Continued monitoring of the fibril heights and morphology reveals further structural changes over time, with little further variation in the ThT binding fluorescence (Fig. 4). Early in the plateau phase (8 h), the majority of fibrils have a height of around 12 nm and a relatively smooth appearance, although the height is observed to vary with a periodicity of 40–70 nm, similar to the "native-like" fibrils produced after a week of standing in Tris buffer at 4 °C (8). Over the course of the following hours and days of incubation at 37 °C, there was a gradual decrease in the mean fibril height, until at 7 days the fibril heights resolved into two peaks, indicating the presence of two distinct fibril types (Fig. 4*D*). (Fitting the combined data to a two-peak Gaussian gives a height of 11.8 ± 0.9 nm for the fibril type that dominates early in the plateau phase, and a height of 9.0 ± 1.2 nm for the fibril type that dominates at

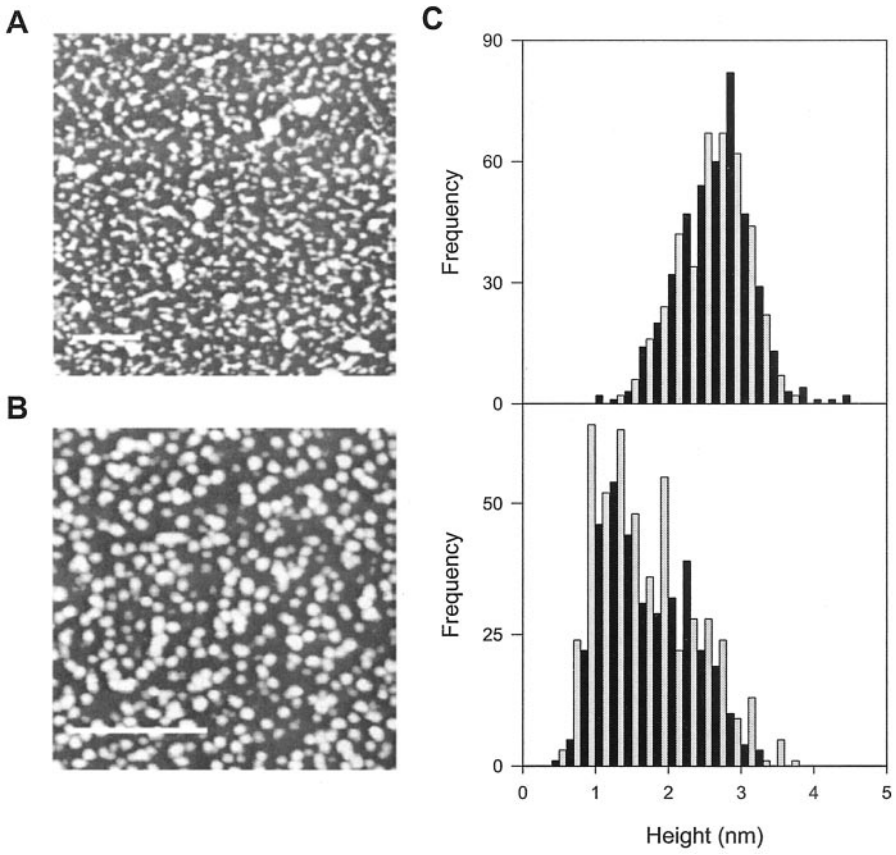

FIG. 3. **AFM characterization of the Ure2 dimer.** AFM height images of Ure2 (*A*) and Δ15–42Ure2 (*B*) in Tris-HCl, pH 8.4, 0.2 M NaCl, room temperature, and 1 μM protein concentration. The *scale bar* represents 200 nm, and the full range of the gray scale corresponding to height was 10 nm. *C*, height distribution of the particles for Ure2 (*black*) and Δ15–42Ure2 (*gray*) at 1 μM protein concentration (*upper panel*) or at approximately 0.1 μM (*lower panel*). In each case the scan area was a 2-μm square or less.

extended incubation times.) The other change that is apparent over this time period is that most fibrils no longer appear smooth, but have a clearly distinguishable twisted or zigzag morphology (Fig. 5*A*). Careful inspection reveals that the small proportion of "twisted" fibrils present at time points when 12-nm fibrils dominate (twisted fibrils indicated by *arrows* in Fig. 5*A*, *8 h*) consistently have heights of around 8 nm. This then indicates that as well as protofilaments, at least two additional types of fibril are present, distinguishable by their height and morphology, the relative proportions of which change over time. The preferential loss of the thicker "smooth" fibrils over time suggests that the twisted fibrils may be derived from the smooth fibrils by conformational conversion or separation of the constituent strands.

Comparison of Fibril Morphology for Ure2, 15Ure2, and Δ15–42Ure2—As described above, a parallel assay by ThT binding and AFM indicates that long fibrils of WT Ure2 are present by the end of the exponential growth phase (Fig. 5*A*, *6 h*), are abundant by early plateau phase (Fig. 5*A*, *8 h*), and persist even at very long incubation times (Fig. 5*A*, *4 d*). Variations in morphology over this time course include a change in the distribution of fibril heights, indicating the progressive appearance of 5-, 8-, 12-, and 9-nm fibrils (Figs. 4*D* and 5*D*). The ThT binding assay (Fig. 2) suggests that 15Ure2, and to a lesser extent Δ15–42Ure2, are also able to form amyloid-like structure, although with a longer nucleation-dependent lag time. A comparison by AFM of WT and mutant fibrils at equivalent stages of the ThT-monitored time course is shown in Fig. 5. Incubation of the proteins was under identical buffer conditions (phosphate buffer, pH 8.0, 37 °C, with shaking), but with the protein concentration of the mutants increased to give a similar kinetic time course as WT. (At lower protein concentrations, similar short fibrils are observed for 15Ure2, but only amorphous structures could be detected for Δ15–42Ure2, data not shown.) The results indicate that the observed increase in ThT binding for the mutant proteins (Fig. 2) coincides with formation of fibrillar structures. However, the mutant fibrils are shorter in length than WT and do not elongate further even at extended incubation times (Fig. 5, *A–C*). This is particularly marked for Δ15–42Ure2, which shows only rod-like structures (150–200-nm length). However, the WT and mutant fibrils or rods show a similar pattern of height changes over time, with progressive appearance of 5-, 8-, 12-, and 9-nm height protofilaments or fibrils (Fig. 5, *D–F*).

Reduced ThT Binding Ability of the Δ15–42Ure2 Mutant—On first inspection, the low level of ThT binding for the Δ15–42Ure2 mutant, particularly in phosphate buffer, appears to correlate with the inability of the fibrils to extend beyond short rods (Fig. 5*C*). However, when investigating Ure2 and its mutants by AFM under "nonaggregating" conditions (Tris, pH 8.4, at 25 °C), we made the unexpected discovery that although WT Ure2 aggregation is strongly reduced under these conditions (16), fibrils of Δ15–42Ure2 are readily formed on standing in this buffer when stored at 4 °C (Fig. 6). WT Ure2 fibrils (Fig. 6, *A* and *D*, *insets* of *E*) formed at 4 °C in this buffer, or at slightly lower pH as used to produce "native-like" Ure2 fibrils (8, 13), are morphologically indistinguishable from these Δ15–42Ure2 fibrils (Fig. 6, *B*, *C*, and *E*). Subpopulations of protofilaments with heights of around 2.5 and 5 nm can be clearly distinguished (Fig. 6, *D* and *E*), and bundling or branching of the filaments can occasionally be observed (Fig. 6*C*). In the high pH buffer, Δ15–42Ure2 fibrils are far more abundant than WT at all time points (Fig. 6*E*). In contrast to the phosphate buffer time course (Fig. 4), few granular particles greater than 4 nm were observed in Tris buffer, suggesting that larger granular particles are not obligate intermediates in fibril formation and that the ThT binding under these conditions is the result of the presence of protofilaments and fibrils.

The contradiction between the extent of ThT binding (Fig. 2*D*) and the abundance of fibrils for Ure2 and Δ15–42Ure2

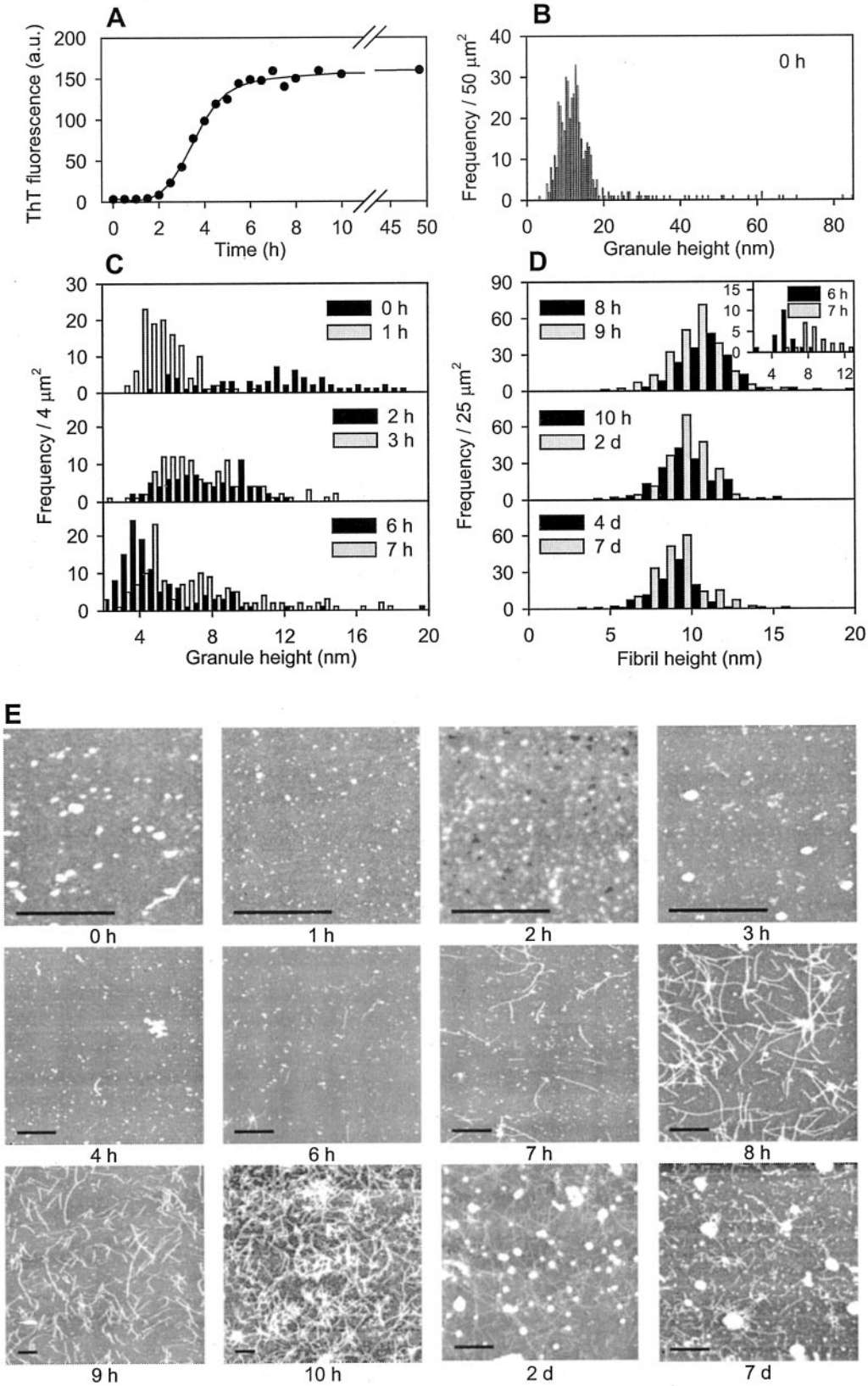

FIG. 4. **Comparison of the time course of formation of amyloid-like structure monitored by ThT binding and AFM.** 30 μM WT Ure2 protein was incubated in sodium/potassium phosphate buffer, pH 8.0, 0.15 M NaCl, and 37 °C with shaking. Structural changes were monitored by ThT binding (*A*) and AFM (*B–E*). *B*, population distribution of heights of granular particles observed in the initial protein sample, derived from analysis of two representative scan areas each of 5 μm square. *C*, population distribution of heights of granular particles observed over different time points, as indicated. All particles detected within a standard, representative scan area of 2 μm square for each hourly time point were included. *D*, population distribution of heights of fibrils observed at different time points, as indicated. A representative 5-μm square scan area from the center of the mica surface was analyzed in each case (but see "Experimental Procedures" and Fig. 6). *E*, AFM height images during the course of fibril formation. Samples were removed from a single reaction vessel at the time points indicated. The *bars* represent 1 μm. The full range of the gray scale corresponding to height was 20, 30, or 40 nm for 0–4 h and 50 nm thereafter, except *2 d*, which was 100 nm.

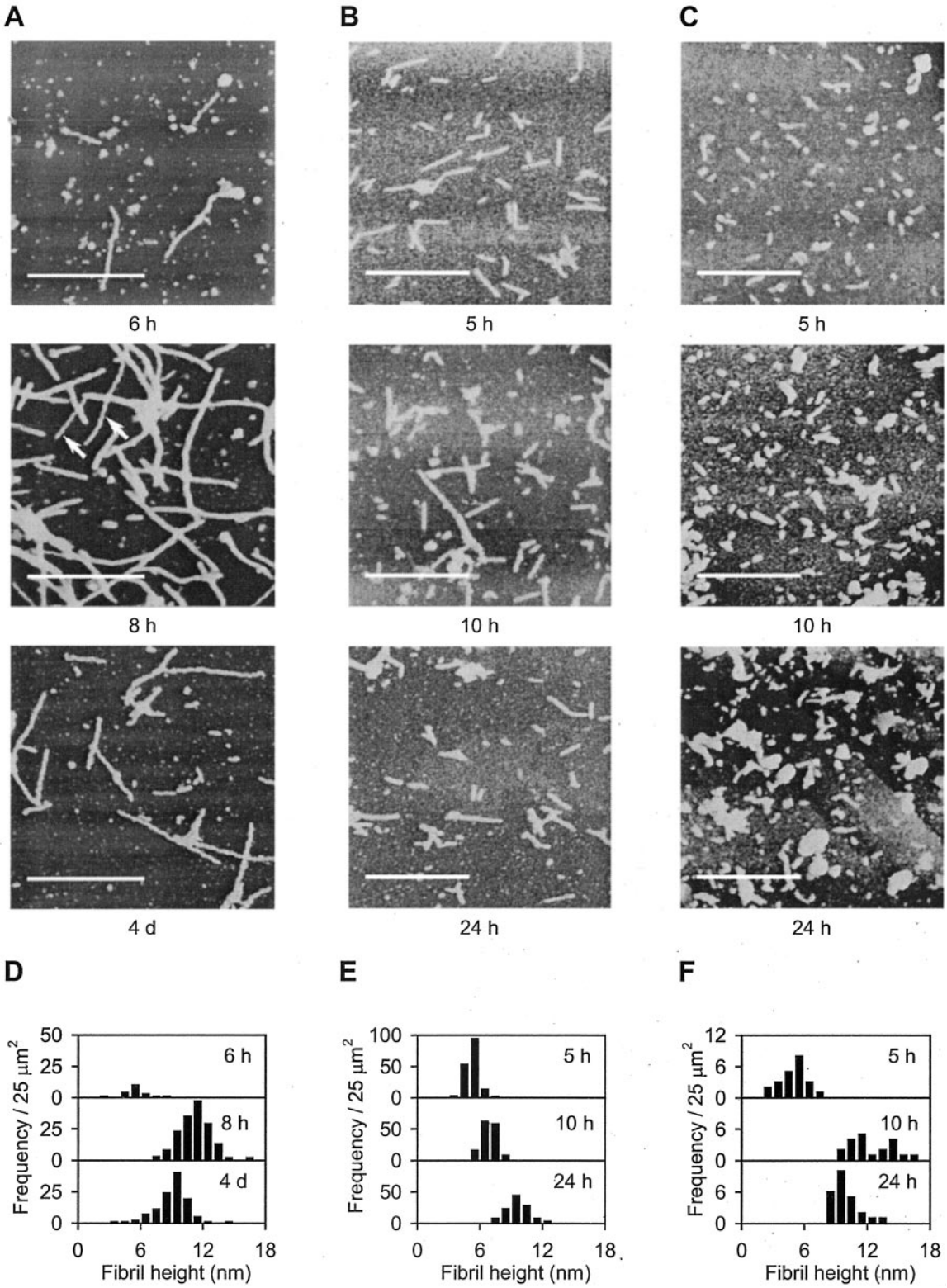

FIG. 5. **Morphology and height distribution of amyloid-like structures monitored by AFM for WT and mutant Ure2.** *A* and *D*, 30 μM WT Ure2; *B* and *E*, 80 μM 15Ure2; and *C* and *F*, 80 μM Δ15–42Ure2. The incubation conditions were the same as in Fig. 4. For each protein, the samples were removed from a single reaction vessel at the time points indicated. *A–C*, AFM height images. The *bar* represents 1 μm. The full range of the gray scale corresponding to height was 30 nm (*B*, *5 h*) or 50 nm (all other panels, *A–C*). *D–F*, population distribution of heights of fibrils or rods at different incubation times as indicated, obtained by measuring the heights of all fibrils within a representative 5-μm square scan area, which included the scan areas displayed in *A–C*.

(Fig. 6*E*) could be the result of a vastly lower affinity of WT Ure2 for the mica surface. However, the lack of WT Ure2 fibrils under these conditions is also apparent from EM (9, 15). The simplest explanation for the discrepancy between ThT binding and the presence of fibrils for Δ15–42Ure2 is that the 15–42 region is important for binding of the hydrophobic dye ThT. Plotting the relative hydrophobicity of the PrD sequence (17, 18) indicates that the region spanning residues 22–34 is rela-

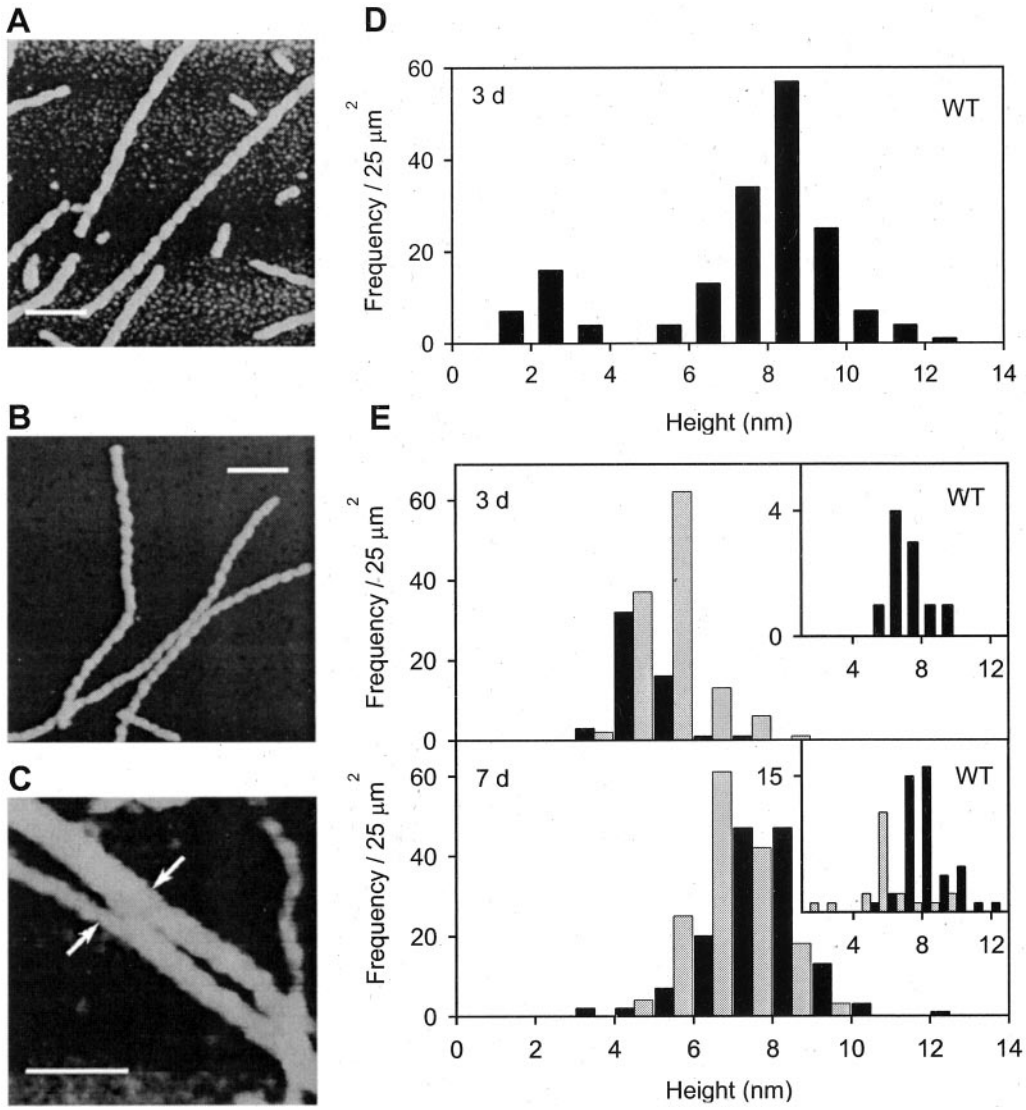

FIG. 6. **Observation of protofilaments and fibrils of WT Ure2 and Δ15–42Ure2.** Incubation was at 4 °C in Tris-HCl buffer, 0.2 M NaCl, pH 8.6 (*A* and *D*) or pH 9.0 (*B*, *C*, and *E*) for 3 or 7 days, as indicated. (Note: the same buffers have a pH of 8.0 or 8.4, respectively, at 25 °C.) *A–C*, the *bar* represents 200 nm, and the full range of the gray scale corresponding to height was 30 nm (*A* and *C*) or 50 nm (*B*). Fibrils of WT (*A*) or Δ15–42Ure2 (*B* and *C*) have a twisted or braided appearance with a height of 8 ± 1 nm and a periodicity of 50–70 nm. *C*, bundling or branching of 5-nm protofilaments into 8-nm fibrils. The height across the junction region (between *arrows*) is 5.0 ± 0.5 nm. *D* and *E*, population distribution of protofilaments and fibrils within representative 5-μm scan areas at the center (*black*) or the edge (*gray*) of the mica surface for WT (*D* and *insets* of *E*) and Δ15–42Ure2 (*E*, *main panels*).

tively hydrophilic. However, two hydrophobic regions consisting of residues 9–21 and 35–43 flank this region (Fig. 1). This may then account for the reduced binding of ThT to the mutant Δ15–42Ure2, despite its ability to form fibrillar structures morphologically indistinguishable from those formed by WT Ure2.

DISCUSSION

The importance of the Ure2 N-terminal domain in prion induction and propagation has been established by genetic studies (2, 40), and the requirement of the PrD to form amyloid-like fibrils *in vitro* has also been demonstrated (5, 15). The mutants initially used in genetic studies to define the PrD were designed at the DNA level, on the basis of convenient endonuclease restriction sites (2, 40), whereas the mutants used in this study were designed at the protein level, based on interesting features of the of the PrD primary structure (Ref. 16 and see Fig. 1). Protein sequence analysis of Ure2 homologs in different species of yeast has recently identified a conserved region in the otherwise divergent PrDs, corresponding to residues 10–40 (44). Within *Saccharomyces* species, the highly conserved region extends from residue 1 to 43. Overexpression of fragments spanning this region causes curing of the prion state in prion strains and inactivation of the Ure2 protein in non-prion strains (44). This suggests that the region spanning residues 1–43 is involved in intermolecular interactions important for formation of the prion state. Our finding that the Ure2 mutants 15Ure2 and Δ15–42Ure2, which have deletions within this crucial region, are nevertheless able to form amyloid-like fibrils is therefore somewhat surprising. Comparison with the Ure2 fragments that have been studied *in vivo* (Table I) would predict that these two mutants would be unable to induce or cure the prion state. Possible explanations for the curing properties of the conserved region when overproduced *in vivo* include a "crystal poisoning mechanism" caused by the interaction of heterogenous molecules with the growing prion seed; induction of chaperones, which then cure the prion state; or the requirement for a cellular cofactor to maintain the prion state, which is depleted by the Ure2 fragment (44, 45). Our *in vitro* results,

TABLE I
Properties of Ure2 mutants and fragments in vivo

Experimental details are given in the references indicated. +, observed; −, not observed (or very low rate of occurrence); ND, not determined; NA, not applicable.

Protein	Curing[a]	Inactivation[b]	Induction[c]	Propagation[d]	Spontaneous generation[e]
Ure2 WT	−	+	+	+	+
Ure2 Δ2–20	−	−	−	ND	ND
Ure2 13–65	−	−	−	ND	NA
Ure2 9–65	+	+	−	ND	NA
Ure2 1–65	+	+	++	+	NA
Ure2 1–80	ND	+	+++	ND	NA
Ure2 1–44	+	+	−	ND	NA
Ure2 1–35	−	−	−	ND	NA
Ure2 Δ1–65	+	−	−	−	ND

[a] Curing of the prion state when the gene is expressed in a WT background in an initially [URE3] prion strain (44, 45).
[b] Inactivation of the Ure2 protein (but not necessarily induction of a stable prion [URE3] state) when the gene is expressed *in vivo* in a WT background (44).
[c] Induction of the [URE3] prion when the gene is expressed in a WT background in an initally non-prion strain (2).
[d] Ability to propagate the prion state when the gene is expressed *in vivo* in a null (*ure2*Δ) background (40).
[e] Spontaneous generation of the [URE3] prion when the gene is expressed *in vivo* in a *ure2*Δ background (40). (This is not applicable to N-terminal fragments that lack the Ure2 functional region because they cannot show the heritable loss of Ure2 function which is the signature of the [URE3] prion.)

TABLE II
Properties of Ure2 mutants in vitro

Exact experimental details are given in the references or figure legends indicated. +, observed; −, not observed; ND, not determined.

Protein	Solubility[a]	Rate of nucleation[b]	ThT binding[c]	Fibril length by AFM[d]
WT Ure2	−	+++	+++	+++
15Ure2	+	+	++	++
Δ15–42Ure2	++	+	+	+
42Ure2	ND	−	−	−
74Ure2	+	ND	ND	ND
90Ure2	+	−	−	−

[a] Solubility in *E. coli* cell extracts (16) or in pure solution (9) in phosphate buffer, pH 7.5. Note that all constructs can be solubilized using Tris-HCl buffer, pH 8.4 (16), and that amyloid-like fibrils of Ure2 PrD fusion proteins have been observed in bacterial cell extracts (7).
[b] Relative rate of nucleation of amyloid-like structure, assayed by ThT binding (+++, shorter lag time; +, longer lag time; −, no increase in ThT binding observed; see Fig. 2).
[c] Relative ThT binding in plateau phase (Fig. 2).
[d] Relative lengths of fibrillar structures detected by AFM after incubation in phosphate buffer (+++, long fibrils; ++, short fibrils; +, rods; −, no fibrils; Figs. 4 and 5). Note that WT and mutant fibrils show the same time-dependent changes in fibril thickness (height) under all conditions and that no differences in fibril length were observed in Tris-HCl buffer (Figs. 5 and 6).

in the absence of cellular cofactors, provide support for a crystal poisoning mechanism and demonstrate the importance of sequence complementarity during self-association to form amyloid-like structure.

The increased lag time for nucleation-dependent formation of amyloid-like structure for the mutants examined in this study is consistent with a role of the conserved region of the Ure2 PrD in forming inter- or intramolecular interactions that help stabilize the prion seed. The low level of binding of the amyloid-specific dye ThT to Δ15–42Ure2, independent of fibril morphology, suggests that the island of normal random sequence within the PrD is involved in formation of the structural motif or binding surface recognized by ThT. This possibly reflects the relatively hydrophobic nature of this region (Fig. 1), which could also explain its involvement in curing and inactivation *in vivo* (Table I). The delayed fibril formation kinetics of the mutants compared with WT provides an explanation for their increased solubility in solution and in *E. coli* cell extracts (Table II). The difference in solubility of WT and mutant Ure2 *in vitro* is most marked in phosphate buffer (16), which correlates with destabilization of the native state relative to partially folded intermediates, likely to be precursors in amyloid formation and other aggregation processes (9). In phosphate buffer, some differences in morphology between WT and mutant Ure2 fibrils could be observed, but this was limited to fibril length. In Tris buffer, WT and mutant fibrils were indistinguishable in length and morphology. Further, under all conditions, the same series of fibrillar intermediates was observed for WT and the mutants. This then implies that the mechanism of assembly of WT and mutant Ure2 fibrils is the same. It will be interesting to test the properties of 15Ure2 and Δ15–42Ure2 *in vivo*, particularly to see whether overproduction of these mutants in a *ure2*Δ background could spontaneously generate a heritable prion-like state, as has been demonstrated for the WT protein (40).

Comparison of the time course of structural changes monitored by ThT binding and by AFM for Ure2 indicates that increased binding of ThT correlates well with appearance of fibrillar structures. However, granular aggregates were also observed under certain conditions and may also bind ThT. Of particular note in the AFM study presented here is the time dependent appearance of a series of Ure2 fibril types, including protofilaments (2–5 nm), intermediate fibrils (8 nm), and two types of mature fibrils (12 and 9 nm), implying a hierarchical mechanism of assembly. Consistent with this, some fibrils had a twisted appearance, and bundling or branching of fibrils could be observed. This is similar to the results obtained for other amyloidogenic proteins (28, 36, 37, 39, 42, 43), including polyglutamine peptides (46). The hierarchical assembly of fibrils, by twisting together of protofilaments or protofibrils to form a variety of fibril morphologies, is emerging as a common mechanism of fibril assembly for all amyloidogenic proteins (47, 48). The yeast prion Sup35, like Ure2, has an N-terminal PrD containing Asn/Gln repeats (49). Fibrils formed from polyglutamine peptides (46, 50, 51), Sup35 (49–52), or Ure2 (5, 6, 14) share many of the tinctorial, structural and mechanistic properties of "typical" amyloids. A striking and unusual property of Ure2, however, is the maintenance of native-like structural and functional properties within the amyloid-like fibrillar arrays (8, 13). Interestingly, fibrils formed by incubation of native, full-length Sup35 show globular appendages radiating from a central fibrillar core under transmission EM (52), highly reminiscent of the "backbone" model proposed for Ure2 fibril assembly (4, 5, 13, 53). Together, these results are consistent with a model for Ure2 fibril formation, in which the PrDs assemble hierarchically into the protofilaments and fibrils of typical amyloid, while still allowing the globular domains to be accommodated in a native-like state.

CONCLUSIONS

A pure solution of either of the mutants 15Ure2 or Δ15–42Ure2 is able to form amyloid-like fibrils morphologically indistinguishable from WT Ure2 but with an increased lag time, whereas 42Ure2 shows no detectable amyloid forming ability. This correlates with the importance of residues 1–43 of the Ure2 N-terminal PrD in mediating prion induction or curing in a WT background *in vivo* (2, 40, 44). The observation of a series of fibrillar intermediates during assembly of Ure2p fibrils supports the existence of a common, hierarchical mechanism for fibril assembly in all amyloidogenic proteins, even where native-like globular structure is accommodated within the fibrillar arrays.

Acknowledgments—We thank Drs. L.S. Itzhaki, X. M. Pan, and L. Serrano for helpful discussions.

REFERENCES

1. Wickner, R. B. (1994) *Science* **264,** 566–569
2. Masison, D. C., and Wickner, R. B. (1995) *Science* **270,** 93–95
3. Prusiner, S. B. (1998) *Proc. Natl. Acad. Sci. U. S. A.* **95,** 13363–13383
4. Speransky, V. V., Taylor, K. L., Edskes, H. K., Wickner, R. B., and Steven, A. C. (2001) *J. Cell Biol.* **153,** 1327–1335
5. Taylor, K. L., Cheng, N., Williams, R. W., Steven, A. C., and Wickner, R. B. (1999) *Science* **283,** 1339–1342
6. Thual, C., Komar, A. A., Bousset, L., Fernandez-Bellot, E., Cullin, C., and Melki, R. (1999) *J. Biol. Chem.* **274,** 13666–13674
7. Schlumpberger, M., Wille, H., Baldwin, M. A., Butler, D. A., Herskowitz, I., and Prusiner, S. B. (2000) *Protein Sci.* **9,** 440–451
8. Bousset, L., Thomson, N. H., Radford, S. E., and Melki, R. (2002) *EMBO J.* **21,** 2903–2911
9. Zhu, L., Zhang, X. J., Wang, L. Y., Zhou, J. M., and Perrett, S. (2003) *J. Mol. Biol.* **328,** 235–254
10. Levine, H. (1993) *Protein Sci.* **2,** 404–410
11. Khurana, R., Uversky, V. N., Nielsen, L., and Fink, A. L. (2001) *J. Biol. Chem.* **276,** 22715–22721
12. Sunde, M., Serpell, L. C., Bartlam, M., Fraser, P. E., Pepys, M. B., and Blake, C. C. (1997) *J. Mol. Biol.* **273,** 729–739
13. Baxa, U., Speransky, V., Steven, A. C., and Wickner, R. B. (2002) *Proc. Natl. Acad. Sci. U. S. A.* **99,** 5253–5260
14. Bousset, L., Briki, F., Doucet, J., and Melki, R. (2003) *J. Struct. Biol.* **141,** 132–142
15. Thual, C., Bousset, L., Komar, A., Walter, S., Buchner, J., Cullin, C., and Melki, R. (2001) *Biochemistry* **40,** 1764–1773
16. Perrett, S., Freeman, S. J., Butler, P. J. G., and Fersht, A. R. (1999) *J. Mol. Biol.* **290,** 331–345
17. Lesser, G. J., and Rose, G. D. (1990) *Proteins* **8,** 6–13
18. Li, X., and Pan, X. M. (2001) *Proteins* **42,** 1–5
19. Coshigano, P. W., and Magasanik, B. (1991) *Mol. Cell. Biol.* **11,** 822–832
20. Galani, D., Fersht, A. R., and Perrett, S. (2002) *J. Mol. Biol.* **315,** 213–227
21. Zhou, J. M., Zhu, L., Balny, C., and Perrett, S. (2001) *Biochem. Biophys. Res. Commun.* **287,** 147–152
22. Zhu, L., Kihara, H., Kojima, M., Zhou, J. M., and Perrett, S. (2003) *Biochem. Biophys. Res. Commun.* **311,** 525–532
23. Perutz, M. F. (1999) *Trends Biol. Sci.* **24,** 58–63
24. Perutz, M. F., Johnston, T., Suzuki, M., and Finch, J. T. (1994) *Proc. Natl. Acad. Sci. U. S. A.* **92,** 6509–6513
25. Perutz, M. F., and Windle, A. H. (2001) *Nature* **412,** 143–144
26. Perutz, M. F., Pope, B. J., Owen, D., Wanker, E. E., and Scherzinger, E. (2002) *Proc. Natl. Acad. Sci. U. S. A.* **99,** 5596–5600
27. Thakur, A. K., and Wetzel, R. (2002) *Proc. Natl. Acad. Sci. U. S. A.* **99,** 17014–17019
28. Bucciantini, M., Giannoni, E., Chiti, F., Baroni, F., Formigli, L. Zurdo, J., Taddei, N., Ramponi, G., Dobson, C. M., and Stefani, M. (2002) *Nature* **416,** 507–511
29. Nucifora, F., Sasaki, M., Peters, M. F., Huang, H., Cooper, J. K., Yamada, M., Takahashi, H., Tsuji, S., Troncoso, J., Dawson, V. L., Dawson, T. M., and Ross, C. A. (2001) *Science* **291,** 2423–2428
30. Chen, S., Berthelier, V., Yang, W., and Wetzel, R. (2001) *J. Mol. Biol.* **311,** 173–182
31. Haass, C., and Steiner, H. (2001) *Nat. Neurosci.* **4,** 859–860
32. Walsh, D. M., Klyubin, I., Fadeeva, J. V., Cullen, W. K., Anwyl, R., Wolfe, M. S., Rowan, M. J., and Selkoe, D. J. (2002) *Nature* **416,** 535–539
33. Uversky, V. N., Li, J., and Fink, A. L. (2001) *J. Biol. Chem.* **276,** 44284–44296
34. Jarrett, J. T., and Lansbury, P. T., Jr. (1993) *Cell* **73,** 1055–1058
35. Kelly, J. W. (2000) *Nat. Struct. Biol.* **7,** 824–826
36. Stine, W. B., Snyder, S. W., Ladror, U. S., Wade, W. S., Miller, M. F., Perun, T. J., Holzman, T. F., and Krafft, G. A. (1996) *J. Protein Chem.* **15,** 193–203
37. Ionescu-Zanetti, C., Khurana, R., Gillespie, J. R., Petrick, J. S., Trabachino, L. C., Minert, L. J., Carter, S. A., and Fink, A. L. (1999) *Proc. Natl. Acad. Sci. U. S. A.* **96,** 13175–13179
38. Naiki, H., Higuchi, K., Hosokawa, M., and Takeda, T. (1989) *Anal. Biochem.* **177,** 244–249
39. Goldsbury, C., Kistler, J., Aebi, U., Arvinte, T., and Cooper, G. J. S. (1999) *J. Mol. Biol.* **285,** 33–39
40. Masison, D. C., Maddelein, M. L., and Wickner, R. B. (1997) *Proc. Natl. Acad. Sci. U. S. A.* **94,** 12503–12508
41. Muller, D. J., Amrein, M., and Engel, A. (1997) *J. Struct. Biol.* **119,** 172–188
42. Harper, J. D., Wong, S. S., Lieber, C. M., and Lansbury P. T., Jr. (1999) *Biochemistry* **38,** 8972–8980
43. Chamberlain, A. K., MacPhee, C. E., Zurdo, J., Morozova-Roche, L. A., Hill, H. A. O., Dobson, C. M., and Davis, J. J. (2000) *Biophys. J.* **79,** 3282–3293
44. Edskes, H., and Wickner, R. B. (2002) *Proc. Natl. Acad. Sci. U. S. A.* **99,** 16384–16391
45. Edskes, H., Gray, V. T., and Wickner, R. B. (1999) *Proc. Natl. Acad. Sci. U. S. A.* **96,** 1498–1503
46. Chen, S., Berthelier, V., Hamilton, J. B., O'Nuallain, B., and Wetzel, R. (2002) *Biochemistry* **41,** 7391–7399
47. Kad, N. M., Myers, S. L., Smith, D. P., Smith, D. A., Radford, S. E., and Thomson, N. H. (2003) *J. Mol. Biol.* **330,** 785–797
48. Khurana, R., Ionescu-Zanetti, C., Pope, M., Li, J., Nielson, L., Ramirez-Alvarado, M., Regan, L., Fink, A. L., and Carter, S. A. (2003) *Biophys. J.* **85,** 1135–1144
49. Serio, T. R., and Lindquist, S. L. (2001) *Adv. Protein Chem.* **59,** 391–412
50. Balbirnie, M., Grothe, R., and Eisenberg, D. S. (2001) *Proc. Natl. Acad. Sci. U. S. A.* **98,** 2375–2380
51. Perutz, M. F., Finch, J. T., Berriman, J., and Lesk, A. (2002) *Proc. Natl. Acad. Sci. U. S. A.* **99,** 5591–5595
52. Glover, J. R., Kowal, A. S., Schirmer, E. C., Patino, M. M., Liu, J. J., and Lindquist, S. (1997) *Cell* **89,** 811–819
53. Baxa, U., Taylor, K. L., Wall, J. S., Simon, M. N., Cheng, N., Wickner, R. B., and Steven, A. C. (2003) *J. Biol. Chem.* **278,** 43717–43727